Bulk band structure of Bi$_2$Te$_3$

Matteo Michiardi,[1] Irene Aguilera,[2] Marco Bianchi,[1] Vagner Eustáquio de Carvalho,[3] Luiz Orlando Ladeira,[3]
Nayara Gomes Teixeira,[3] Edmar Avellar Soares,[3] Christoph Friedrich,[2] Stefan Blügel,[2] and Philip Hofmann[1]

[1]*Department of Physics and Astronomy, Interdisciplinary Nanoscience Center, Aarhus University, 8000 Aarhus C, Denmark*
[2]*Peter Grünberg Institute and Institute for Advanced Simulation, Forschungszentrum Jülich and JARA, D-52425 Jülich, Germany*
[3]*Departamento de Física, ICEx, Universidade Federal de Minas Gerais, 30123-970 Belo Horizonte, MG, Brazil*

The bulk band structure of Bi$_2$Te$_3$ has been determined by angle-resolved photoemission spectroscopy and compared to first-principles calculations. We have performed calculations using the local density approximation (LDA) of density functional theory and the one-shot GW approximation within the all-electron full-potential linearized augmented-plane-wave (FLAPW) formalism, fully taking into account spin-orbit coupling. Quasiparticle effects produce significant changes in the band structure of Bi$_2$Te$_3$ when compared to LDA. Experimental and calculated results are compared in the spectral regions where distinct differences between the LDA and GW results are present. Overall a superior agreement with GW is found, highlighting the importance of many-body effects in the band structure of this family of topological insulators.

I. INTRODUCTION

In the last few years topological insulators have been the subject of extensive studies, both experimental and theoretical [1,2]. For these materials, the peculiarity of having a bulk band parity inversion in an odd number of time-reversal invariant momenta across the Brillouin zone (BZ) gives rise to the existence of topological surface states protected by time-reversal symmetry [3]. The surface states crossing the band gap are necessarily metallic and present spin helicity, a condition where the electrons' spin is locked to their momentum, opening the possibility of applications in spintronics. While many topological insulators have been predicted and experimentally investigated, the bismuth chalcogenides are by far the most extensively studied.

For experimental studies, Bi$_2$Se$_3$ and Bi$_2$Te$_3$ are considered to be prototypical materials [4–6]. They share the same rhombohedral crystal structure, which consists of quintuple layers bound to each other through weak van der Waals forces, giving easy access to the (111) surface by cleavage. Their surface electronic structure is also very similar in the sense that both support a single closed surface Fermi contour around the $\bar{\Gamma}$ point of the (111) surface BZ. In both cases, this is caused by a parity inversion at the bulk Γ point. However, while the surface electronic properties are similar, there are some significant differences in the detailed dispersion of the surface states. Both materials show a warping of the surface state Dirac cone far away from the Dirac point, but for Bi$_2$Te$_3$ this warping is much more pronounced than for Bi$_2$Se$_3$ [6–9].

These materials also show significant differences in their bulk electronic structure. For instance, as was recently shown via a comparison between angle-resolved photoemission (ARPES) measurements and GW calculations [10,11], Bi$_2$Se$_3$ has a direct band gap with the bulk valence band maximum (VBM) and conduction band minimum (CBM) located at the Γ point of the BZ, whereas the character of the band gap in Bi$_2$Te$_3$ is still subject to debate [12–14].

So far, *ab initio* calculations for topological insulators have been mainly performed using either the local density (LDA) or generalized gradient (GGA) approximations of density

functional theory (DFT). The reason is that LDA and GGA constitute an efficient approach which allows for the study not only of the bulk but also of the surface states. Since the parity inversion in the bulk states is mainly caused by spin-orbit coupling (SOC) effects, including these proved to be crucial. LDA and GGA calculations of the surface states have mostly shown good agreement with the experimental results [4,15]. However, these two approaches fail to correctly describe some important aspects of the bulk band structures. Vidal *et al.* [16] have demonstrated that LDA may incorrectly predict trivial insulators as topological insulators. In addition, several GW studies of topological insulators in the last few years [10–12,14,16–20] have shown that the nature of the band gap (indirect or direct), its magnitude, and the effective masses of the bands involved in the band inversion are not described correctly within LDA but are often corrected with the GW approximation.

As an example, LDA predicts Bi$_2$Se$_3$ to be an indirect gap semiconductor with the VBM close to the Z point [4,11], whereas the inclusion of a GW correction correctly reproduces the direct band gap, in agreement with experiments [10,11]. Such details are also crucial for the surface electron dynamics as they determine if the surface states are degenerate with bulk states at another $k_\parallel$ or not. In fact, reaching the topological transport regime [21] would not be possible for Bi$_2$Se$_3$ as described by LDA, but it is possible in the case where the Dirac point lies within the direct band gap at $\bar{\Gamma}$ [10].

Calculations using the GW approach were also able to reproduce more subtle details in the experimentally observed dispersion. The first GW bulk band structure of Bi$_2$Se$_3$ showed that the band-inversion-induced characteristic M-shaped dip in the band forming the VBM disappears upon the inclusion of GW corrections [11]. Again, this is in good agreement with the results from ARPES for a cut exactly through the Γ point but not for a cut at a different $k_\perp$ value in the Γ-Z direction (for a good illustration of this, see the supporting material of Ref. [22]). Also using the GW approximation, Nechaev *et al.* were later able to show that the M-shaped dip reappears for larger $k_\perp$, as seen in the bulk bands projected onto the (111)-surface BZ [10].

In addition to the *a posteriori* observation that GW is in general in better agreement with ARPES experiments than LDA, a comparison between GW and ARPES is also more justified from a fundamental point of view. LDA is meant to predict ground-state properties and not excitation energies; GW, on the other hand, is constructed to describe the energies required to remove an electron from or add an electron to the system (the quasiparticle energies), in clear correspondence to the excitation energies measured in direct and inverse photoemission experiments.

In order to assess the accuracy of the LDA and GW approximations for Bi_2Te_3, we present bulk band structures of this topological insulator obtained in LDA and GW calculations and compare them with band structure measurements by ARPES. Particular emphasis is put on the differences between the LDA and GW results in the regions where these can be directly tested experimentally.

II. METHODS

The Bi_2Te_3 crystal was grown in two steps. First, the stoichiometric compound was synthesized by heating the pure elements (Bi and Te) in an ampoule at about 300 °C in a hydrogen environment to eliminate oxidized species. On suite, the ampoule was evacuated at room temperature and then heated to 200 °C for 24 hours and then up to 587 °C at a rate of 0.5 °C/min and left there for three hours. The system was then cooled down at 0.2 °C/min in 72 hours. At this point, the obtained products were checked by x-ray diffraction and the synthesis of the compound was confirmed. In a second step, the single crystal was grown by heating the obtained compound inside an evacuated and sealed quartz ampoule up to 271 °C at 0.5 °C/min and kept at this value for two hours. The temperature was then increased to 587 °C at a rate of 2 °C/min and the ampoule was left at this temperature for 24 hours. The system was then cooled down to room temperature at 0.05 °C/min. The grown single crystal was then characterized by Laue diffraction. The impurity level was measured by x-ray photoelectron spectroscopy for different emission angles from the sputtered (111) surface. At all angles, only Bi_2Te_3-related peaks have been found and the impurity level is thus below the detection limit ($\approx 1\%$). The Seebeck coefficient was measured and its value (191.6 μ V/K) was found to be in good agreement with published results for high-quality Bi_2Te_3crystals [23].

ARPES measurements of the band dispersion of Bi_2Te_3 were performed on the SGM-3 beamline of the ASTRID synchrotron radiation facility [24]. The Bi_2Te_3 single crystals were cleaved in vacuum at room temperature and successively measured at $\sim$70 K. ARPES spectra have been acquired at different photon energies, spanning from 14 eV to 32 eV. The crystals have been aligned in two different high symmetry directions: $\bar{\Gamma}$-$\bar{M}$ and $\bar{\Gamma}$-$\bar{K}$. The energy and angular resolution for ARPES measurements were better than 20 meV and 0.2°, respectively.

ARPES is the standard technique to obtain the dispersion of the bulk band structure of solids and has been applied to many materials [25,26]. The key problem in this is that the wave vector component perpendicular to the surface $k_\perp$ is not conserved in the photoemission process, in contrast to the component parallel to the surface $k_\parallel$. Band structure

determinations are therefore often restricted to the direction that corresponds to normal emission from the sample surface, i.e., for $k_\parallel = 0$. The initial state's $k_\perp$ is not known but the high-symmetry line it lies on is known. Therefore, extrema in the dispersion can be identified as critical point energies in the band structure. We make extensive use of this idea, extending it to other values of $k_\parallel$. If one is interested in the detailed dispersion of the states between the critical points, one has to assume a certain final state dispersion, for example a free electron final state [25]. If this is not accurate, this only affects the details of the dispersion in between the critical points but not the critical point energies. Here we mainly make use of free electron final states to conveniently display the photoemission data as two-dimensional intensity plots. Note that the photon energies used (14–32 eV) provide, for electrons close to the Fermi level, strongly surface sensitive information as the mean free path of the photoelectrons is very small. This is not known to affect the observed dispersion of the bulk initial states as the tails of these states near the surface are excited. In fact, the ARPES determination of the bulk band structure has been used for numerous materials, also some with large unit cells. It was, for instance, possible to determine the splitting for the buried bilayers in the high-temperature superconductor Bi2212 [27]. In Bi_2Se_3, which has the same geometric structure as Bi_2Te_3, good quantitative agreement in the analysis of bulk properties was achieved comparing ARPES and bulk sensitive Haas-van Alphen oscillations [28], as well as ARPES and *ab initio* calculations [10]. Using moderate energy ARPES it has even been possible to observe states that are buried deep below the surface if only an evanescent tail of the wave function is present within the mean free path of the photoelectrons [29].

The LDA and GW calculations were performed with the all-electron FLAPW codes FLEUR [30] and SPEX [31], respectively. We used the experimental lattice structure of Ref. [32]. For the LDA calculations, we employed an angular momentum cutoff for the muffin-tin spheres of $l = 10$ and a plane-wave cutoff in the interstitial region of 4.5 bohr^{-1}. The SOC was incorporated self-consistently employing the second-variation technique [33]. We used the same basis for the wave functions in the GW calculations and, furthermore, employed an angular momentum cutoff of $l = 5$ and a linear momentum cutoff of 2.9 bohr^{-1} for the representation of the screened interaction and related quantities [31,34]. For the calculation of the bulk band structure in the Γ-Z-F-Γ-L path, we have used a $4 \times 4 \times 4$ **k**-point mesh for the screened interaction W and evaluated the quasiparticle energies on 190 **k** points along the path. However, for the band structure projected onto the (111) surface (in the $\bar{\Gamma}$-$\bar{M}$ and $\bar{\Gamma}$-$\bar{K}$ directions), we had to calculate self-energy corrections for almost 2000 extra **k** points (no interpolation technique was employed). In order to save computation time, we resorted to a $2 \times 2 \times 2$ **k**-point set for W in this case. Tests show that the quasiparticle energies differ by maximally 50 meV between calculations with a $2 \times 2 \times 2$ and a $6 \times 6 \times 6$ sampling, whereas, for most of the **k** points, the differences are much smaller, in particular for the Γ and Z points (0.6 and 14 meV, respectively). Therefore, $2 \times 2 \times 2$ turns out to give enough accuracy for the purpose of this work. We have included 500 bands and semicore d states of Bi and Te. In addition, to have an accurate description of high-lying states and to avoid linearization errors [35–37], we

have included two local orbitals per angular momentum up to $l = 3$ for each atom.

In contrast to most GW calculations that include spin-orbit interactions, we take the SOC already into account in the reference system [17] instead of in an *a posteriori* correction, employing the four-component spinor wave functions. The self energy thus acquires terms that couple the two spin channels, enabling a many-body renormalization of the SOC itself (for a detailed discussion see Ref. [38]).

As in Ref. [20], we solve the quasiparticle equation in the basis of the LDA single-particle states explicitly. This takes the off-diagonal elements of the self energy into account, allowing for changes in the quasiparticle wave functions, which proved to be critical, for example, to describe the highest valence band of Bi$_2$Te$_3$ correctly [20]. Although still being a one-shot approach, we go beyond the usual *perturbative* solution of the quasiparticle equation of motion, in which the quasiparticle wave functions are approximated by the corresponding LDA single-particle states, which requires only the diagonal elements of the self energy to be calculated. In Ref. [14], it was concluded that studies beyond the perturbative one-shot approach were required for Bi$_2$Te$_3$, as the dependence on the one-particle starting point was found to be stronger than for Bi$_2$Se$_3$.

For a comparison to the ARPES results, the theoretical Fermi level has been adjusted (shifting it up from mid gap by 0.13 eV) so as to match at best the measured upper valence band. This procedure is justified because of the strong intrinsic n doping of the crystals. It is fair to assume that the bulk band dispersion obtained here is not affected by the increased bulk carrier concentration that stems from the doping. There is little evidence of such an effect taking place in other semiconductors, and studies on doped Bi$_2$Se$_3$ in particular show that, even with strong bulk or surface doping, the bands are merely rigidly shifted [22,39,40].

III. RESULTS AND DISCUSSION

The calculated bulk band structure of Bi$_2$Te$_3$ is shown in Fig. 1(a) for both the LDA and GW approaches. Figures 1(b) (LDA) and 1(c) (GW) show the bulk bands projected onto the (111)-surface BZ along the $\bar{\Gamma}$-$\bar{K}$ and $\bar{\Gamma}$-$\bar{M}$ directions. The LDA band structures are in good agreement with previous publications [4,14,41,42]. Note that the band projections in Figs. 1(b) and 1(c) are not slab calculations of the surface electronic structure. Therefore, they do not show the topological surface state nor any other surface states that might be present in the projected band gaps.

The LDA calculation [Fig. 1(b)] shows an almost-direct fundamental gap of 50 meV with both the VBM and CBM in the $\bar{\Gamma}$-$\bar{M}$ direction. The GW approximation [Fig. 1(c)] confirms the position of the VBM in $\bar{\Gamma}$-$\bar{M}$, but places the CBM in the Γ-Z direction instead, giving an indirect band gap of 120 meV, in better agreement with experimental values (130–170 meV, Refs. [43–46]). The VB exhibits the characteristic M-shaped dispersion (darker solid lines) around $\bar{\Gamma}$ which is symptomatic of the band inversion at Γ. The transition from LDA to GW results in a flattening of the M-shape dip. As shown by $k \cdot p$ perturbation theory in the case of Bi$_2$Se$_3$ in Ref. [11], this effect stems from the band
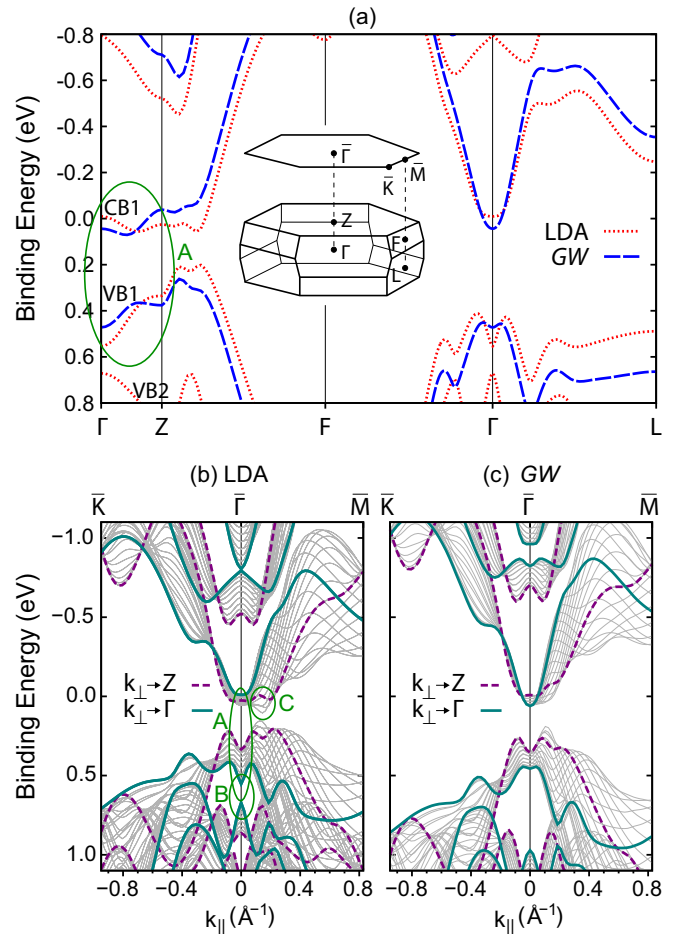

FIG. 1. (Color online) (a) Bulk band dispersion of Bi$_2$Te$_3$ calculated by LDA (dotted red line) and GW (long-dashed blue line). VB1, VB2, and CB1 denote the bands for which the dispersion is compared to the experimental data. The inset shows the bulk Brillouin zone and its projection onto the (111) surface. (b) and (c) Bulk bands projected onto the (111) surface along the $\bar{\Gamma}$-$\bar{K}$ and $\bar{\Gamma}$-$\bar{M}$ directions calculated with LDA and GW, respectively. The darker solid and dashed lines correspond to paths including the Γ and Z point, respectively. The green ovals denote the regions **A**, **B**, and **C** that were chosen for a comparison to the experimental data because the differences between LDA and GW are largest there. The binding energy scales in the calculations have been shifted by 0.13 eV in order to facilitate the comparison with experiment.

inversion due to SOC: GW increases the band gap with respect to LDA for all **k** points (as it happens for most trivial gaps) but reduces the gap at Γ because it is here inverted. The inclusion of quasiparticle effects "flattens" the band even though the band inversion persists [20].

It should be noted that the dispersion of the highest valence band in the present GW calculation [Fig. 1(a)] and the one by Yazyev *et al.* in Ref. [11] differ significantly. In particular, the M shape which is flattened but persists in our case almost disappears in Ref. [11]. These discrepancies have been recently found in Ref. [38] to be due to the *a posteriori* inclusion of SOC in Ref. [11]. Furthermore, we do not employ a pseudopotential approximation, nor a plasmon-pole model in our calculations.
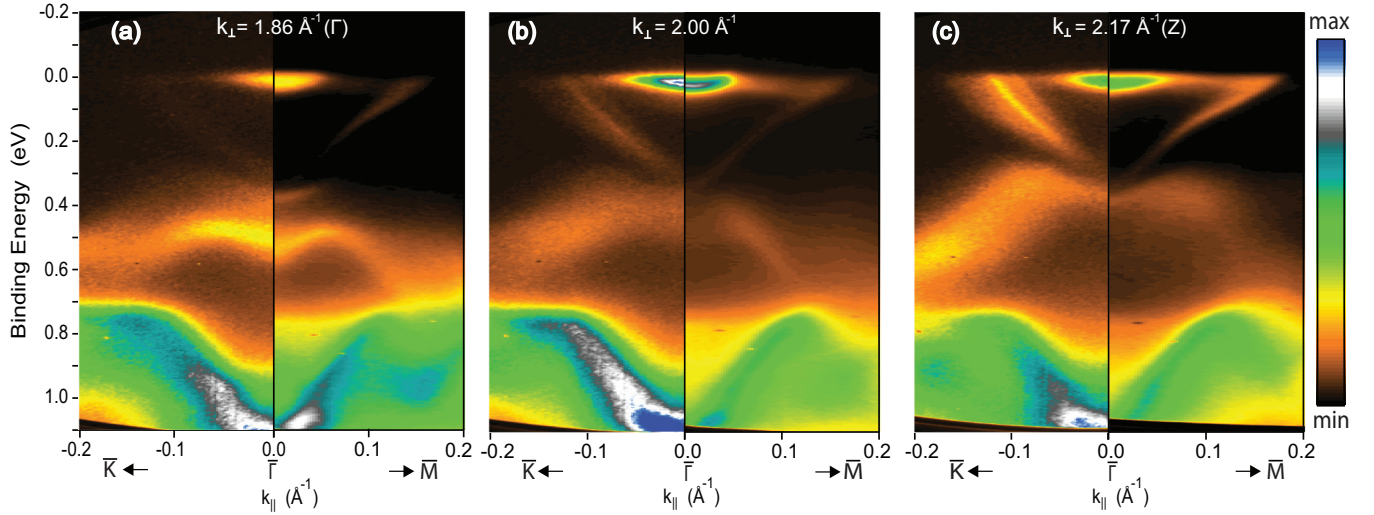
FIG. 2. (Color online) (a)–(c) Photoemission intensity from $Bi_2Te_3(111)$ along the $\bar{K}$-$\bar{\Gamma}$ and $\bar{\Gamma}$-$\bar{M}$ directions for different values of the crystal momentum perpendicular to the surface $k_\perp$.

It is interesting to notice that the band structure of Bi_2Te_3 shows pronounced differences to that of the analog compound Bi_2Se_3. The Bi_2Se_3 band structure, investigated by ARPES and GW, reveals the VBM to be precisely at the Γ point [10]. The flattening of the M shape is in fact much stronger and restores the convex shape to the upper valence band. Since the CBM is also found at Γ this results in the debated direct band gap. This does not seem to happen in Bi_2Te_3 because of a qualitative difference in the bulk-projected bands: In the case of Bi_2Te_3 [Figs. 1(b) and 1(c)], the highest occupied state at $\bar{\Gamma}$ is at the Z point, whereas in the case of Bi_2Se_3 it is placed at the Γ point. This implies that the disappearance of the M shape is really affecting the highest occupied state in Bi_2Se_3 (and therefore it changes the nature of the fundamental band gap) but not in Bi_2Te_3.

In Figs. 1(b) and 1(c), when LDA and GW results are compared, there are three features that show larger differences between the two approaches. These three features are shown enclosed by green ovals and are labeled **A**, **B**, and **C**. **A** refers to the differences in the binding energies at Γ and Z and the detailed dispersion along the Γ-Z direction. **B** labels the region of a projected band gap in the occupied states. This gap is significantly smaller in LDA. Finally, **C** points out the difference in the CBM's location. In LDA, this is found along the $\bar{\Gamma}$-$\bar{M}$ while GW places it at $\bar{\Gamma}$. This is also relevant for the nature of the band gap. In the comparison to the ARPES spectra, we focus the discussion on these three regions.

Figure 2 shows parts of a large set of photon-energy-dependent ARPES data; the photoemission intensity along $\bar{K}$-$\bar{\Gamma}$ and $\bar{\Gamma}$-$\bar{M}$ is shown for three different photon energies. The data have been converted from the raw format (intensity as a function of kinetic energy and emission angle) to the intensity as a function of binding energy and $k_\parallel$. The relative intensity of the bands is different for the two measured directions, such that intensity jumps occur at $k_\parallel = 0$ for some binding energies. This is ascribed to polarization-dependent matrix elements in the photoemission process. In fact, the color range is scaled separately on the two sides of the respective intensity

maximum. Note that it is not possible to estimate the width of the bands by a mere inspection of the color figures. Indeed, this is not even easy to do within one side. Several features are immediately identified in these spectra: The conduction band is clearly discernible at the Fermi level and $k_\parallel \approx 0$. This is expected due to the strong n doping of the samples. The topological surface state with its characteristic Dirac-cone shape is visible between the conduction band and the valence band. As expected for a two-dimensional state, it does not disperse with $k_\perp$. The top of the valence band shows a clear dispersion with photon energy. Finally a very intense state can be seen at high binding energy. This state does not present any dispersion with $k_\perp$ either.

Figure 3 shows the photoemission intensity in normal emission extracted from a large number of such images as a function of binding energy and $k_\perp$, the component of the crystal momentum perpendicular to the surface. As mentioned
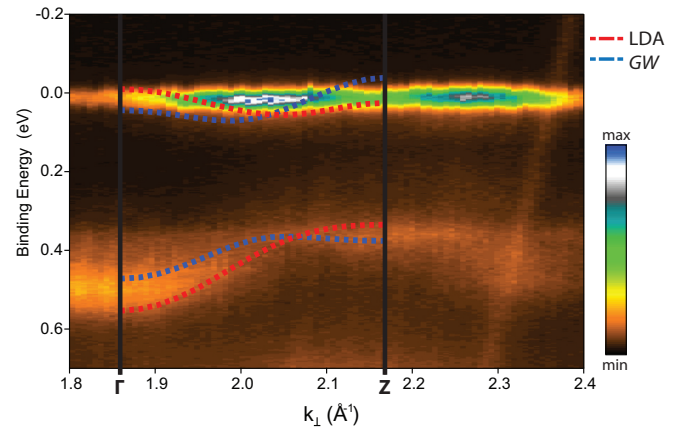

FIG. 3. (Color online) Photoemission intensity in normal emission as a function of $k_\perp$, i.e., the dispersion along the Γ-Z direction with superimposed bands calculated with the LDA (red dashed line) and the GW approximation (blue dashed line). The position of the bulk Γ and Z points is marked.

above, $k_\perp$ is not conserved in the photoemission process and the conversion from photon energy to $k_\perp$ therefore requires assumptions about the final states in the photoemission process. Here we assume free-electron-like final states such that $k_\perp = \sqrt{2m_e/\hbar^2}[V_0 + E_{\mathrm{kin}}\cos^2(\theta)]^{1/2}$, where θ is the electron's emission angle and V_0 is the inner potential [25]. The inner potential needs to be chosen such that the location of the observed critical points in the dispersion agrees with the expected position along $k_\perp$, i.e., with the critical points placed either at the Γ or at the Z point of the bulk BZ. In the data, a clear dispersion of the top valence band is seen and, guided by the band structure calculation along Γ-Z, we determine $V_0 = 1.0$ eV, such that the high binding-energy extremum of the band is placed at the Γ point. Note that this value of the inner potential is quite different from that for Bi$_2$Se$_3$ where V_0 is approximately 11.8 eV [5,10]. This is not surprising because the bulk band structures of the two compounds are, in fact, rather different despite their structural similarity. This is already clear from the entirely different dispersion of the topmost valence band seen here. Also note that the inner potential is essentially a fitting parameter used to localize the high symmetry points in the $k_\perp$ direction, and we merely use it to conveniently display the ARPES data in a two-dimensional intensity plot. An inaccurate assignment of the inner potential would therefore merely "squeeze" or "stretch" the dispersion between two critical points but it would not affect the overall trend of the dispersion and, therefore, our conclusions.

We compare the results of the calculations with the experiment in the three spectral regions **A**–**C** where there are clear differences between the LDA and GW results.

A: Note that comparing the detailed calculated band dispersion to the experimental results is not without problems because $k_\perp$ is not conserved in the photoemission process and our simple assumption of free-electron final state might not be justified. Nevertheless, if we restrict the comparison to normal emission, the observed states lie along the Γ-Z direction (in the absence of surface umklapp processes), greatly simplifying the analysis. Figure 3 shows a comparison of the two calculated band dispersions for the Γ-Z direction and the experimental data in the region of the lowest conduction band CB1 and highest valence band VB1.

For VB1, the predicted dispersion in the Γ-Z shows a binding-energy maximum at Γ and a binding-energy minimum at Z, and this ordering has also been used to guide the choice of the inner potential V_0 for the free electron final state. The main difference between the LDA result and the GW result is that the bandwidth is larger in LDA. When comparing this to the experimental data in Fig. 3, it appears that the experimental bandwidth lies in between the LDA and GW results. Another difference between the two theoretical approaches is that the GW dispersion shows a small dip in the vicinity of the Z point, which is not present in LDA. The experimental result does show this small dip in agreement with GW.

For the lowest conduction band CB1, LDA and GW both predict the binding-energy maximum to be located in between the high symmetry points (at $k_\perp = 2.06$ Å^{-1} and 1.99 Å^{-1}, respectively). It should be noted that the dispersion obtained by a GW calculation where the SOC is included *a posteriori* [see, e.g., Figs. 1(b) and 2(b) in Refs. [38] and [11], respectively]
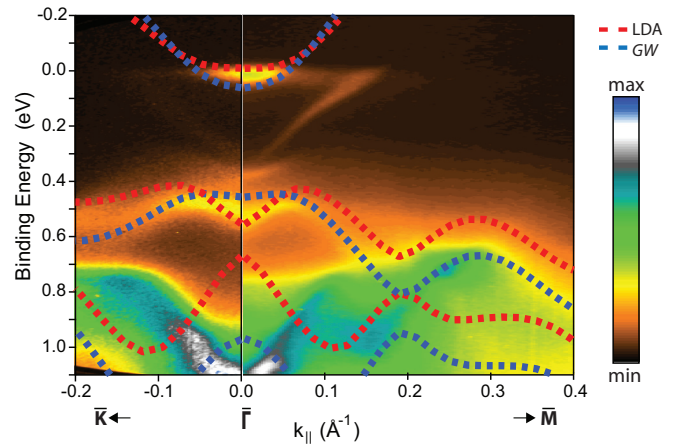

FIG. 4. (Color online) (a) Photoemission intensity for $k_\perp$ near the bulk Γ point along the $\bar{\mathrm{K}}$-$\bar{\Gamma}$-$\bar{\mathrm{M}}$ direction with the LDA (red dashed line) and GW bands (blue dashed line).

does not show any binding-energy maximum of CB1 in between Γ and Z. As evident in Fig. 3, the LDA bandwidth is smaller, so that the band has a noticeably higher binding energy at Z in LDA than in GW. A careful inspection of the experimental data appears to confirm the prediction of a binding-energy maximum in between Γ and Z, with CB1 apparently reaching a maximum at $k_\perp = 2.035$ Å^{-1}. Far from this maximum, we can only detect the tail of the CB1 because it disperses above the Fermi level. Since the photoemission matrix elements can have an important role in the spectral intensity profile for different photon energies and CB1 never disperses very clearly below the Fermi level, it remains unclear whether the CB1 band has a higher binding energy at Γ, in agreement with GW, or at Z, as predicted by LDA.

B: The spectral region of the projected band gap between VB1 and VB2 near $\bar{\Gamma}$ is distinctly different in the LDA and GW calculations. In LDA, the gap is much narrower at $\bar{\Gamma}$ because of the smaller gap between VB1 and VB2 at the bulk Γ point. Further towards $\bar{\mathrm{M}}$ and $\bar{\mathrm{K}}$, the lower edge of the gap is determined by the VB2 dispersion close to the bulk Z point [dashed lines in Fig. 1(b) and 1(c)]. Experimentally, one might be able to distinguish between the two scenarios by following the dispersion of the VB1 and VB2 bands. Such a comparison close to the bulk Γ point is shown in Fig. 4. As in the data of Fig. 2, VB1 is easily identifiable in the spectra whereas VB2 is not. Instead, one finds a very intense V-shaped feature in the binding-energy region of VB2, as also seen in Figs. 2(a)–2(c). We assign this feature to a surface state in the projected band gap between VB1 and VB2. This is confirmed by the fact that the state's dispersion is independent of $k_\perp$, something that is already apparent in Figs. 2(a)–2(c) and confirmed by fitting the dispersion at different photon energies. The absence of VB2 features in the investigated energy range implies that the projected band gap at $\bar{\Gamma}$ must be quite wide, significantly wider than predicted by LDA. Surface calculations within LDA [41,47,48] have indicated the existence of a similar V-shaped surface state in Bi$_2$Se$_3$ and Sb$_2$Te$_3$ but not in Bi$_2$Te$_3$ [15,41]. For this latter material, the surface states show a wrong dispersion (W shaped) due to the W shape of the too small LDA bulk projected gap.

The existence and dispersion of the surface state, and the absence of bulk states in this region, thus strongly favors the presence of a larger projected band gap, in agreement with the GW result. However, the projected band gap is likely to be even wider than predicted by GW. The VB2 does not fall within the spectral range investigated near Γ in Fig. 4, but, as predicted by GW [dashed line in Fig. 1(c)], it can be observed around Z [as a blue feature in Fig. 2(c)] at $k_\parallel \approx -0.17$ Å^{-1} off-normal emission and approximately 0.9 eV of binding energy. While the quasiparticle correction, in fact, yields a considerably larger gap than LDA, it still seems to underestimate the experimental one. Self-consistent GW calculations might be able to improve the agreement with experiment.

C: A final distinct difference between the LDA and GW results is the position of the CBM. As seen in Figs. 1(b) and 1(c), the GW bands show the projected CBM to be placed at $\bar{\Gamma}$ whereas the LDA calculation shows the CB1 dropping below the value at $\bar{\Gamma}$ for $k_\parallel = 0.145$ Å^{-1} along the $\bar{\Gamma}$-$\bar{M}$ direction with the highest binding energy at $k_\perp = 2.108$ Å^{-1}. Such a signature of a CBM off the $\bar{\Gamma}$ point is never observed in the experiment. To illustrate this, Fig. 5(a) shows a spectrum along the $\bar{M}$-$\bar{\Gamma}$-$\bar{M}$ direction for $k_\perp = 2.108$ Å^{-1}. Clearly, the experimental results cannot be reconciled with the CB1 dispersion predicted by LDA while they are more consistent with the GW result. Figure 5(b) shows the photoemission intensity in the $\bar{\Gamma}$-$\bar{M}$ direction at $k_\parallel = 0.145$ Å^{-1} as a function of binding energy and $k_\perp$, i.e., along a line parallel to the Γ-Z line. The $k_\perp$ components of the two points marked as A ($k_\parallel = 0.145$ Å^{-1}, $k_\perp = 1.86$ Å^{-1}) and B ($k_\parallel = 0.145$ Å^{-1}, $k_\perp = 2.17$ Å^{-1}) correspond to those of the Γ and Z point, respectively. A single, nondispersing feature is observed and assigned to the topological surface state. A drop of the CB1 below the Fermi level, as predicted by LDA, is not seen for any value of $k_\perp$ between A and B.
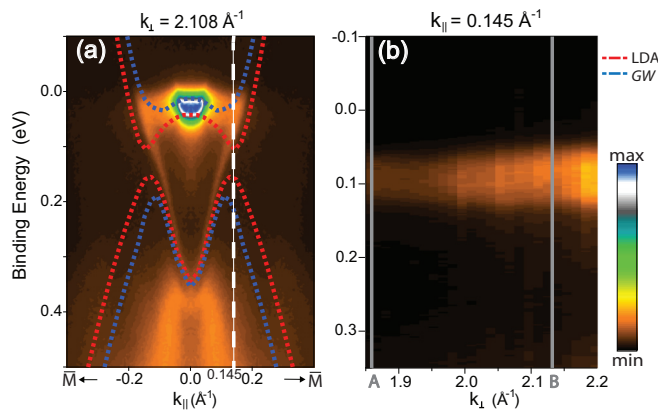
The position of the absolute CBM as well as of the VBM in Bi_2Te_3 is still a subject of debate [12–14]. Our measurements show that the CBM is placed along Γ-Z. This clearly excludes the possibility of a direct gap since the VBM is off $\bar{\Gamma}$. This can be seen from the M-shaped valence band branches which reach the lowest binding energy at $k_\parallel \neq 0$ (see Fig. 2). Both LDA and GW agree in placing the VBM along $\bar{\Gamma}$-$\bar{M}$. According to LDA, this will create an almost-direct band gap with the CBM as mentioned before. In the case of GW the VBM is found nearly in the same position as for LDA, but it gives rise to the indirect band gap. While both approaches predict the VBM along $\bar{\Gamma}$-$\bar{M}$, the experimental result does not confirm this clear directional preference. We find that the energies of the two local binding-energy minima along $\bar{\Gamma}$-$\bar{M}$ and $\bar{\Gamma}$-$\bar{K}$, respectively at $k_\perp \sim 1.97$ Å^{-1} and $k_\perp \sim 2.16$ Å^{-1}, are actually very similar.

As mentioned above, the VBM is predicted both in LDA and GW to be placed in the $\bar{\Gamma}$-$\bar{M}$ direction, specifically, for the $k_\perp$ shown in Fig. 5(a). However, the binding energy of this maximum is somewhat larger in the experiment in better agreement with GW than with LDA. The GW calculation has thus acted again as correcting the LDA in the right direction. We would like to point out that the widely used *perturbative* one-shot GW approach (i.e., calculating only the diagonal elements of the self energy) has been shown to be wrong in this direction of the BZ [see Fig. 5(b) of Ref. [14] and its discussion]. This is a clear case of unsatisfactory quasiparticle dispersions, which is caused by the neglect of hybridization effects that arise from the off-diagonal part of the self energy [20].

IV. CONCLUSIONS

We have analyzed the LDA and GW band structures of Bi_2Te_3 and compared them to ARPES measurements. In particular, we have analyzed in detail three regions of the spectra in which qualitative differences between LDA and GW are observed.

We have also discussed the position of the VBM and CBM and the nature of the gap. The LDA calculation shows an almost direct gap of 50 meV with both the VBM and CBM in the $\bar{\Gamma}$-$\bar{M}$ direction. The GW approximation confirms the position of the VBM along $\bar{\Gamma}$-$\bar{M}$ but places the CBM in the Γ-Z direction instead, giving an indirect band gap of 120 meV, in better agreement with experimental values (130–170 meV, Refs. [43–46]). Our ARPES results confirm the position of the CBM along Γ-Z, as predicted by GW and the position of the VBM away from the $\bar{\Gamma}$ point. However, the valence band does not reach noticeably smaller binding energies along $\bar{\Gamma}$-$\bar{M}$ than along $\bar{\Gamma}$-$\bar{K}$.

The one-shot GW calculations including the off-diagonal elements of the self energy [20] and a consistent treatment of spin-orbit interactions [38] constitute a significant overall improvement to the LDA results and produce quasiparticle band structures in better agreement with ARPES measurements. This (together with the recent findings [10,11] about the direct gap of Bi_2Se_3) emphasizes the importance of many-body effects on the band structure of this family of topological insulators.

FIG. 5. (Color online) (a) Photoemission intensity along the $\bar{M}$-$\bar{\Gamma}$-$\bar{M}$ direction for the $k_\perp$ value for which LDA predicts the CBM. LDA and GW bands are shown as red and blue dashed lines, respectively. (b) Photoemission intensity for the $k_\parallel$ value of the LDA CBM as a function of binding energy and $k_\perp$. The corresponding $k_\parallel$ value is marked in (a) by a vertical dashed line. We define the points A and B as the projections of Γ and Z on the $k_\parallel = 0.145$ Å^{-1} line. The only discernible feature is caused by the topological surface state.

ACKNOWLEDGMENTS

[1] J. Moore, Nat. Phys. **5**, 378 (2009).

[2] M. Z. Hasan and C. L. Kane, Rev. Mod. Phys. **82**, 3045 (2010).

[3] L. Fu and C. L. Kane, Phys. Rev. B **76**, 045302 (2007).

[4] H. Zhang, C.-X. Liu, X.-L. Qi, X. Dai, Z. Fang, and S.-C. Zhang, Nat. Phys. **5**, 438 (2009).

[5] Y. Xia, D. Qian, D. Hsieh, L. Wray, A. Pal, H. Lin, A. Bansil, D. Grauer, Y. S. Hor, R. J. Cava, and M. Z. Hasan, Nat. Phys. **5**, 398 (2009).

[6] Y. L. Chen, J. G. Analytis, J. H. Chu, Z. K. Liu, S. K. Mo, X. L. Qi, H. J. Zhang, D. H. Lu, X. Dai, Z. Fang, S. C. Zhang, I. R. Fisher, Z. Hussain, and Z.-X. Shen, Science **325**, 178 (2009).

[7] L. Fu, Phys. Rev. Lett. **103**, 266801 (2009).

[8] K. Kuroda, M. Arita, K. Miyamoto, M. Ye, J. Jiang, A. Kimura, E. E. Krasovskii, E. V. Chulkov, H. Iwasawa, T. Okuda, K. Shimada, Y. Ueda, H. Namatame, and M. Taniguchi, Phys. Rev. Lett. **105**, 076802 (2010).

[9] M. Bianchi, R. C. Hatch, Z. Li, P. Hofmann, F. Song, J. Mi, B. B. Iversen, Z. M. Abd El-Fattah, P. Löptien, L. Zhou, A. A. Khajetoorians, J. Wiebe, R. Wiesendanger, and J. Wells, ACS Nano **6**, 7009 (2012).

[10] I. A. Nechaev, R. C. Hatch, M. Bianchi, D. Guan, C. Friedrich, I. Aguilera, J. L. Mi, B. B. Iversen, S. Blügel, Ph. Hofmann, and E. V. Chulkov, Phys. Rev. B **87**, 121111 (2013).

[11] O. V. Yazyev, E. Kioupakis, J. E. Moore, and S. G. Louie, Phys. Rev. B **85**, 161101 (2012).

[12] E. Kioupakis, M. L. Tiago, and S. G. Louie, Phys. Rev. B **82**, 245203 (2010).

[13] B. Y. Yavorsky, N. F. Hinsche, I. Mertig, and P. Zahn, Phys. Rev. B **84**, 165208 (2011).

[14] I. A. Nechaev and E. V. Chulkov, Phys. Rev. B **88**, 165135 (2013).

[15] A. Herdt, L. Plucinski, G. Bihlmayer, G. Mussler, S. Döring, J. Krumrain, D. Grützmacher, S. Blügel, and C. M. Schneider, Phys. Rev. B **87**, 035127 (2013).

[16] J. Vidal, X. Zhang, L. Yu, J.-W. Luo, and A. Zunger, Phys. Rev. B **84**, 041109 (2011).

[17] R. Sakuma, C. Friedrich, T. Miyake, S. Blügel, and F. Aryasetiawan, Phys. Rev. B **84**, 085144 (2011).

[18] A. Svane, N. E. Christensen, M. Cardona, A. N. Chantis, M. van Schilfgaarde, and T. Kotani, Phys. Rev. B **84**, 205205 (2011).

[19] Z. Zhu, Y. Cheng, and U. Schwingenschlögl, Phys. Rev. Lett. **110**, 077202 (2013).

[20] I. Aguilera, C. Friedrich, G. Bihlmayer, and S. Blügel, Phys. Rev. B **88**, 045206 (2013).

[21] D. Hsieh, Y. Xia, D. Qian, L. Wray, J. H. Dil, F. Meier, J. Osterwalder, L. Patthey, J. G. Checkelsky, N. P. Ong, A. V. Fedorov, H. Lin, A. Bansil, D. Grauer, Y. S. Hor, R. J. Cava, and M. Z. Hasan, Nature (London) **460**, 1101 (2009).

[22] M. Bianchi, D. Guan, S. Bao, J. Mi, B. B. Iversen, P. D. C. King, and P. Hofmann, Nat. Commun. **1**, 128 (2010).

[23] J. P. Fleurial, L. Gailliard, R. Triboulet, H. Scherrer, and S. Scherrer, J. Phys. Chem. Solids **49**, 1237 (1988).

[24] S. Hoffmann, C. Søndergaard, C. Schultz, Z. Li, and P. Hofmann, Nucl. Instrum. Methods Phys. Res., Sect. A **523**, 441 (2004).

[25] F. J. Himpsel, Appl. Opt. **19**, 3964 (1980).

[26] S. Hüfner, *Photoelectron Spectroscopy*, 3rd ed. (Springer, Berlin, 2003).

[27] Y. D. Chuang, A. D. Gromko, A. Fedorov, Y. Aiura, K. Oka, Y. Ando, H. Eisaki, S. Uchida, and D. S. Dessau, Phys. Rev. Lett. **87**, 117002 (2001).

[28] J. G. Analytis, J.-H. Chu, Y. Chen, F. Corredor, R. D. McDonald, Z. X. Shen, and I. R. Fisher, Phys. Rev. B **81**, 205407 (2010).

[29] J. A. Miwa, P. Hofmann, M. Simmons, and J. Wells, Phys. Rev. Lett. **110**, 136801 (2013).

[30] http://www.flapw.de.

[31] C. Friedrich, S. Blügel, and A. Schindlmayr, Phys. Rev. B **81**, 125102 (2010).

[32] R. W. G. Wyckoff, *Crystal Structures 2* (J. Wiley and Sons, New York, 1964).

[33] C. Li, A. J. Freeman, H. J. F. Jansen, and C. L. Fu, Phys. Rev. B **42**, 5433 (1990).

[34] T. Kotani and M. van Schilfgaarde, Solid State Commun. **121**, 461 (2002).

[35] C. Friedrich, A. Schindlmayr, S. Blügel, and T. Kotani, Phys. Rev. B **74**, 045104 (2006).

[36] C. Friedrich, M. C. Müller, and S. Blügel, Phys. Rev. B **83**, 081101(R) (2011); **84**, 039906(E) (2011).

[37] G. Michalicek, M. Betzinger, C. Friedrich, and S. Blügel, Comput. Phys. Commun. **184**, 2670 (2013).

[38] I. Aguilera, C. Friedrich, and S. Blügel, Phys. Rev. B **88**, 165136 (2013).

[39] S. Xu, M. Neupane, C. Liu, D. Zhang, A. Richardella, L. Andrew Wray, N. Alidoust, M. Leandersson, T. Balasubramanian, J. Sanchez-Barriga, O. Rader, G. Landolt, B. Slomski, J. Hugo Dil, J. Osterwalder, T. Chang, H. Jeng, H. Lin, A. Bansil, N. Samarth, and M. Zahid Hasan, Nat. Phys. **8**, 616 (2012).

[40] Y. L. Chen, J.-H. Chu, J. G. Analytis, Z. K. Liu, K. Igarashi, H. H. Kuo, X. L. Qi, S. K. Mo, R. G. Moore, D. H. Lu, M. Hashimoto, T. Sasagawa, C. Zhang, I. R. Fisher, Z. Hussain, and Z. X. Shen, Science **329**, 659 (2010).

[41] S. Eremeev, Y. Koroteev, and E. Chulkov, JETP Lett. **91**, 387 (2010).

[42] O. V. Yazyev, J. E. Moore, and S. G. Louie, Phys. Rev. Lett. **105**, 266806 (2010).

[43] I. G. Austin, Proc. Phys. Soc. London **72**, 545 (1958).

[44] C. Li, A. L. Ruoff, and C. W. Spencer, J. Appl. Phys. **32**, 1733 (1961).

[45] R. Sehr and L. R. Testardi, J. Phys. Chem. Solids **23**, 1219 (1962).

[46] G. A. Thomas, D. H. Rapkine, R. B. V. Dover, L. F. Mattheiss, W. A. Sunder, L. F. Schneemeyer, and J. V. Waszczak, Phys. Rev. B **46**, 1553 (1992).

[47] L. Plucinski, A. Herdt, S. Fahrendorf, G. Bihlmayer, G. Mussler, S. Doring, J. Kampmeier, F. Matthes, D. E. Burgler, D. Grutzmacher *et al.*, J. Appl. Phys. **113**, 053706 (2013).

[48] C. Pauly, G. Bihlmayer, M. Liebmann, M. Grob, A. Georgi, D. Subramaniam, M. R. Scholz, J. Sánchez-Barriga, A. Varykhalov, S. Blügel, O. Rader, and M. Morgenstern, Phys. Rev. B **86**, 235106 (2012).